Journal of Catalysis 269 (2010) iii–vii

Contents lists available at ScienceDirect

Journal of Catalysis

journal homepage: www.elsevier.com/locate/jcat

Journal of Catalysis Vol. 269, Issue 2, 2010

Contents

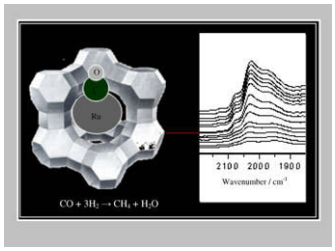

The removal of CO in hydrogen rich containing feed gas via selective methanation was studied on two differently supported Ru catalysts. The kinetic activity is shown to be dependent on the amount of linearly adsorbed CO on Ru acting as active species.

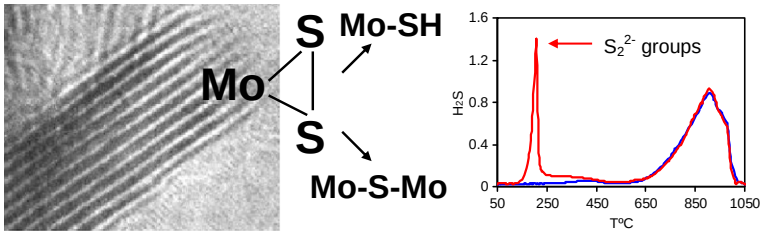

Over-stoichiometric sulfur present at the edges of MoS_2 in the form of S_2^{2-} moieties plays a crucial role for the HDS activity and HYD selectivity, as well as for the promotion of unsupported MoS_2 catalysts by nickel and cobalt.

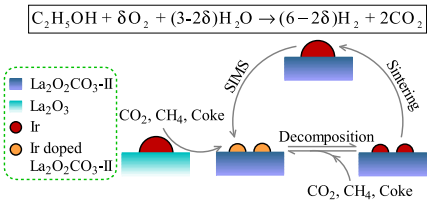

Ir nanoparticles are *in situ* formed and dispersed over $La_2O_2CO_3$-II through the strong interaction between metal and support during the course of oxidative steam reforming of ethanol.

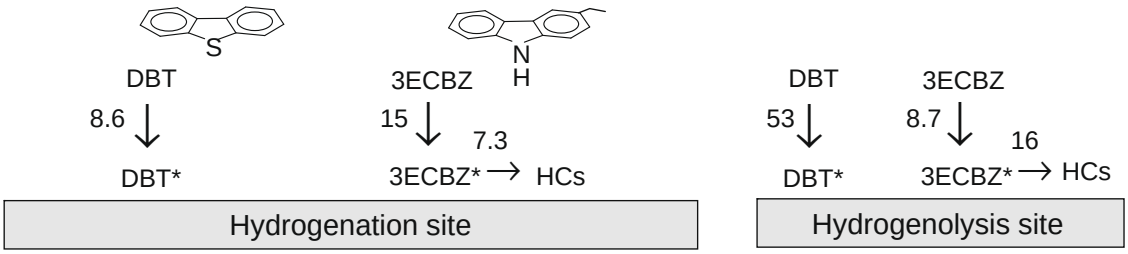

Shown here are relative adsorption constants for dibenzothiophene and 3-ethylcarbazole and relative rate constants for hydrodenitrogenation of 3-ethylcarbazole to hydrocarbons. Dibenzothiophene hydrodesulfurization is less inhibited by 3-ethylcarbazole on the hydrogenolysis sites.

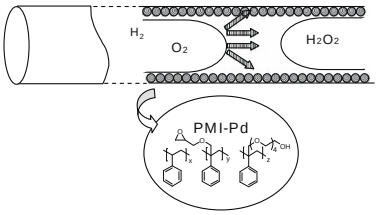

The direct formation of hydrogen peroxide from H_2 and O_2 was successfully carried out in a capillary microreactor under ambient conditions using palladium nanoparticles incarcerated in an amphiphilic polystyrene-based polymer.

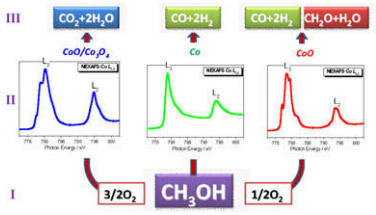

Methanol oxidation on cobalt: the relation between the gas phase composition (I), the cobalt oxidation state (II) and the dominant reaction paths (III), observed by combined *on-line* mass spectrometry (QMS) and in situ X-ray absorption spectroscopy (XAS). The X-ray absorption spectra of Co $L_{3,2}$ edge were obtained on a cobalt crystal under reaction mixture at 520 K, using different methanol-to-oxygen mixing ratios.

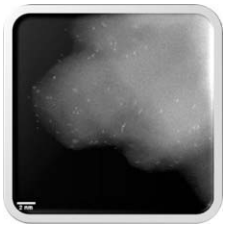

Aberration-corrected STEM images and EXAFS and IR spectra demonstrate that site-isolated iridium complexes are the predominant species in an MgO-supported catalyst used for ethene hydrogenation; the scattering centers indicate individual Ir atoms and clusters of several Ir atoms.

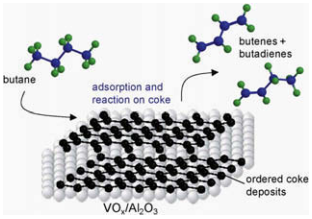

Carbonaceous material deposited on VO_x/Al_2O_3 is shown to provide the catalytically active sites for *n*-butane dehydrogenation at 973 K. The activity of carbon is confirmed through studies on carbon nanofibres.

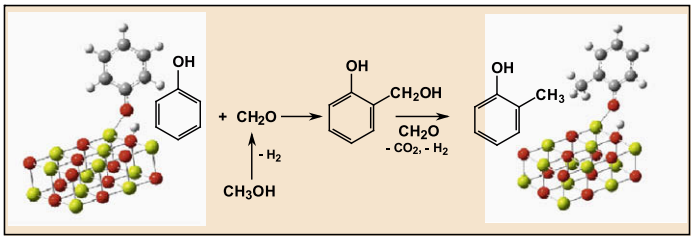

The mechanism of the gas-phase methylation of phenol with methanol, catalyzed by basic systems, is not a conventional electrophilic ring-substitution by the activated alcohol, but instead proceeds via the intermediate formation of formaldehyde and the regio- and chemo-selective ortho-hydroxymethylation of the phenolic ring by the aldehyde.

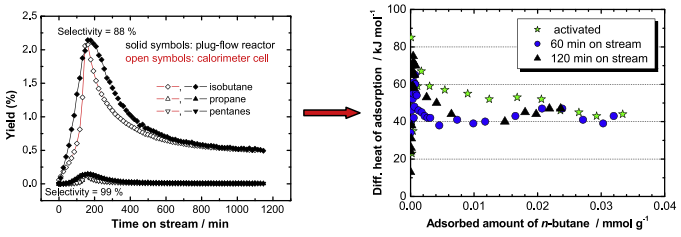

A calorimeter cell was used as a flow reactor to generate an active sulfated zirconia catalyst. Differential heats of butane adsorption measured subsequently in situ indicate that a small fraction of sites is altered as the catalyst changes its performance.

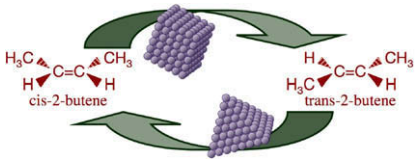

Colloidal chemistry was used to make catalysts consisting of cubic and tetrahedral platinum nanoparticles dispersed on silica supports. It was shown how this control on catalyst shape can be used to direct selectivity in catalytic olefin isomerization reactions.

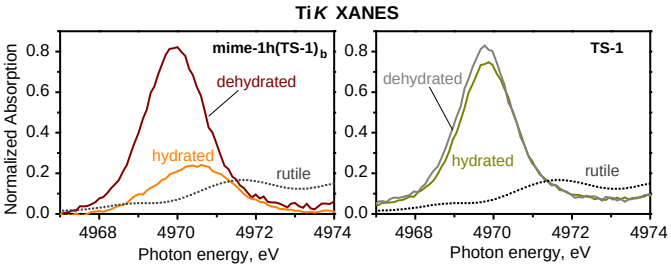

Characterization of ordered mesoporous solids synthesized from TS-1 seeds confirmed microporosity in mesopore walls. Highly accessible Ti sites in hydrophilic environment explain spectacular epoxidation activities with cyclohexene and complete failure with *n*-hexene.

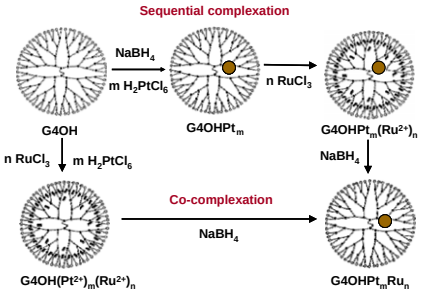

Pt–Ru dendrimer-metal nanocomposites were synthesized using co-complexation and sequential complexation methods as shown. The Pt–Ru bimetallic catalysts synthesized via dendrimer route were found to exhibit different structural properties and catalytic performance (i.e., activities, selectivities) for selective hydrogenation when compared to conventionally prepared Pt–Ru samples.

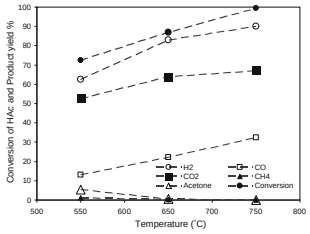

The performance of ceria–zirconia-supported Ni and Rh catalysts is investigated in steam reforming of acetic acid. High hydrogen yields and very low rates of carbonaceous depositions are observed over the Rh catalyst.

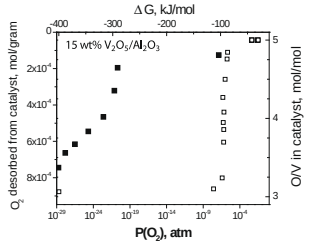

V_2O_5/Al_2O_3 catalysts with different redox properties exhibited a similar activity for methanol selective oxidation suggesting that oxygen removal from the surface is not the rate-limiting step for this reaction.

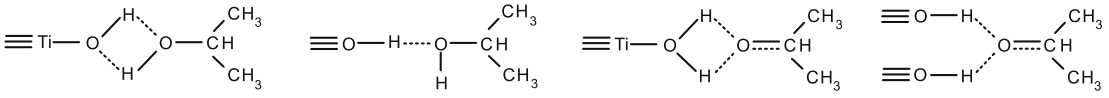

Kinetic studies revealed that photocatalytic oxidation of acetone and isopropanol in aqueous systems is susceptible to changes in the Brönsted acid/base character of TiO_2 caused by changes in pH.

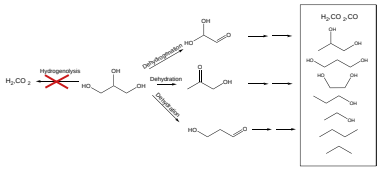

Glycerol is catalytically converted in aqueous phase over Pt/Al_2O_3 via bifunctional pathways involving dehydrogenation, dehydration and decarboxylation/decarbonylation. C—C and C—O bond hydrogenolysis does not occur.

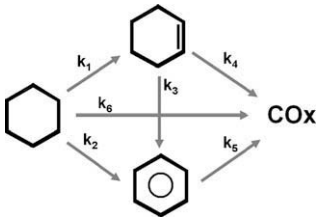

In the oxidative dehydrogenation of cyclohexane by highly uniform vanadium oxide on alumina catalysts, the activity of vanadia polymers was higher than monomers for every reaction in the network (k_2–k_6) except for the formation of cyclohexene (k_1) where the activity of monomers was higher.